Journal Pre-proofs

Support Effects in Iridium-Catalyzed Aerobic Oxidation of Benzyl Alcohol Studied by Modulation-Excitation Attenuated Total Reflection IR Spectroscopy

Shizuka Ito, Xianwei Wang, Ammara Waheed, Gao Li, Nobutaka Maeda, Daniel.M. Meier, Shuichi Naito, Alfons Baiker

PII: S0021-9517(20)30456-5
DOI: https://doi.org/10.1016/j.jcat.2020.11.010
Reference: YJCAT 13969

To appear in: *Journal of Catalysis*

Received Date: 19 August 2020
Revised Date: 28 October 2020
Accepted Date: 6 November 2020

Please cite this article as: S. Ito, X. Wang, A. Waheed, G. Li, N. Maeda, Daniel.M. Meier, S. Naito, A. Baiker, Support Effects in Iridium-Catalyzed Aerobic Oxidation of Benzyl Alcohol Studied by Modulation-Excitation Attenuated Total Reflection IR Spectroscopy, *Journal of Catalysis* (2020), doi: https://doi.org/10.1016/j.jcat.2020.11.010

Support Effects in Iridium-Catalyzed Aerobic Oxidation of Benzyl Alcohol Studied by Modulation-Excitation Attenuated Total Reflection IR Spectroscopy

Shizuka Ito [a,b1], *Xianwei Wang* [c,1], *Ammara Waheed* [a,b], *Gao Li* [a,b], *Nobutaka Maeda* [d]*, *Daniel. M. Meier* [d], *Shuichi Naito* [e], *Alfons Baiker* [f]*

[a] Gold Catalysis Research Center, State Key Laboratory of Catalysis, Dalian Institute of Chemical Physics, Chinese Academy of Sciences, 457 Zhongshan Road, Dalian 116023, China

[b] University of Chinese Academy of Sciences, Beijing 100049, China.

[c] Key Laboratory of Industrial Ecology and Environmental Engineering, School of Environmental Science and Technology, Dalian University of Technology, Dalian 116024, China

[d] Institute of Materials and Process Engineering, Zurich University of Applied Sciences (ZHAW), Technikumstrasse 9, CH-8400 Winterthur, Switzerland.

[e] Department of Material and Life Chemistry, Faculty of Engineering, Kanagawa University, 3-27-1, Rokkakubashi, Kanagawa-ku, Yokohama, 221-8686 Japan

[f] Institute for Chemical and Bioengineering, Department of Chemistry and Applied Biosciences, ETH Zurich, Hönggerberg, HCI, CH-8093 Zurich, Switzerland

[1] These authors contributed to this work equally.

*Corresponding authors: maeo@zhaw.ch (N.M.); alfons.baiker@chem.ethz.ch (A.B.)

Highlights

- Supports strongly influence Ir-catalysed oxidation of benzyl alcohol (BA)
- ATR-IR-MES spectroscopy facilitated the detection of adsorbed transient alkoxide
- Dissociative adsorption of BA and formation of alkoxide species is crucial
- Adsorbed alkoxide is key intermediate for high catalytic performance.
- Atypical catalytic behaviour of Ir/TiO_2 in SMSI state has been examined

Abstract

The influence of the support (Al_2O_3, CeO_2, TiO_2) in the oxidation of benzyl alcohol (BA) to benzaldehyde on Ir-based catalysts was investigated by ATR-IR spectroscopy in tandem with modulation excitation spectroscopy (ATR-IR-MES) at working conditions of the catalysts. ATR-IR-MES unveiled the dissociative adsorption of BA and the formation of adsorbed transient alkoxy species ($C_6H_5CH_2O$-) to be key for high catalytic performance. These species were detected on Ir/TiO_2 and Ir/Al_2O_3 but not on Ir/CeO_2, which exhibited poor catalytic performance. On Ir/TiO_2 pretreated with hydrogen at 450^{o}C about 84% of the Ir sites were blocked due to formation of a titania overlayer. However, this catalyst afforded a more than seven times higher activity than the corresponding one pretreated at 300^{o}C, where about 68% of the Ir sites were blocked. The high activity of the titania overlayer is attributed to the formation of Ti cations with oxygen vacancies caused by the hydrogen pretreatment.

Keywords: aerobic oxidation, benzyl alcohol, iridium catalysts, ATR-IR spectroscopy, modulation excitation spectroscopy, effect of supports, Al_2O_3, CeO_2, transient alkoxide, TiO_2 overlayer.

1. Introduction

The importance of carbonyl compounds like ketones and aldehydes in chemical industry has spurred research interests in both industry and academia. Carbonyl compounds are normally produced by oxidation of corresponding alkanes and alcohols [1]. A major issue that industries are facing is the massive amounts of wastes often produced in case of noncatalytic stoichiometric reactions, such as toxic oxidants, by-products and heavy metals [2]. To tackle all these issues, heterogeneously catalyzed oxidation processes are mostly considered to be more environmentally benign [1,2].

The catalytic oxidation of alcohols with molecular oxygen has been widely studied focusing on the active metals, oxide supports, reaction conditions, and reaction mechanisms [2-4]. As an environmentally clean technology, the oxidation needs to be performed under mild conditions (low temperature and pressure), but for economic reasons kept at high conversion and selectivity. Among the various supported metal catalysts applied for the selective oxidation of alcohols with molecular oxygen, the most prominent are those based on Pd [5-10], Au [11-16], Ag [17,18], and Pt [19-21]. Alloying of Pd and Pt with Au has been shown to greatly

improve the performance of the corresponding monometallic catalysts [16, 22-27]. Besides all these catalysts, various other catalysts have been reported to exhibit moderate or even excellent behavior, particularly supported iridium [28-30], hydrotalcites, and hydrotalcite supported catalysts [31].

Benzaldehyde (BAL) is a valuable product or intermediate for the synthesis of various fine chemicals and pharmaceuticals. Its production by aerobic oxidation of benzyl alcohol (BA) has been the subject of many investigations since BA is also a suitable model substrate for studying the aerobic oxidation of primary aromatic alcohols.

Among the noble metals investigated, iridium catalysts have received relatively little attention so far, albeit they were shown to afford a selectivity to BAL up to > 99 % at high conversion of BA [28,29]. TiO_2 as support of Ir particles outperformed any other metal oxides supports (e.g. SiO_2, Al_2O_3, CeO_2 etc.) in terms of both conversion and selectivity [28]. Interestingly, Ir/TiO_2 catalysts pretreated with H_2 at higher temperatures showed the best catalytic performance even though most of the Ir surface was covered by partially reduced Ti oxides due to strong-metal-support-interaction (SMSI) [29, 32].

In several studies attenuated total reflection infrared spectroscopy (ATR-IR) has been used to gain insight into the surface processes occurring during aerobic oxidation of benzyl alcohol on Pd-based catalysts, mainly focusing on undesired side reactions [33-39].

Here we applied in situ ATR-IR in tandem with modulation excitation spectroscopy (MES) and phase sensitive detection (PSD) to shed light on the surface processes occurring at the catalytic solid-liquid interfaces of differently supported Ir catalysts with the aim to uncover how the different supports affect the catalytic behavior of these catalysts. ATR-IR-MES spectra attained at working conditions of the catalysts revealed that the presence of adsorbed alkoxide (benzyloxy-species) is crucial for achieving high catalytic performance. Reasons for the outstanding catalytic behavior of TiO_2-supported Ir catalysts, particularly for the atypical behavior of Ir/TiO_2 catalysts pretreated in hydrogen, are examined.

2. Experimental

2.1. Catalyst preparation

The catalysts consisting of Ir nanoparticles deposited on different supports were prepared by a conventional wet-impregnation method using H_2IrCl_6 (WAKO, 36.5 % aqueous solution) as Ir precursor and TiO_2, CeO_2 , and Al_2O_3 (all from Nippon Aerosil Co., Ltd.) as metal oxide supports, as described elsewhere [28,29]. The loading amount of Ir was adjusted to 5wt%. The as-prepared samples were dried overnight at 100 ^oC and then pretreated with pure hydrogen at

300 °C for 3 h. Preliminary tests showed that lower Ir-content are advantageous for the investigation of the influence of the SMSI on the catalytic behavior due to stronger effect. Therefore, 2 wt% Ir/TiO_2 catalysts were prepared for this purpose. For this study the impregnated samples were dried at 100 °C and then pretreated with pure H_2 flow at varying temperature (300 °C, 450 °C and 600 °C) for 3 h.

2.2. Catalyst Characterization

TEM images were taken on a FEI Tecnai G^2 F30 microscope operated at 200 kV. The catalyst powders pretreated by H_2 were mounted onto a carbon-coated Pt grid, which was then placed in the TEM column. Particle size distributions were based on analyzing 50 particles per sample.

The specific surface areas of all catalysts were determined by nitrogen adsorption measurements at 77 K on an ASAP 2020 apparatus (Micromeritics) applying the Brunauer-Emmett-Teller (BET) method. Prior to adsorption measurements, all samples were degassed at 150 °C for 4 h to remove adsorbed CO_2 and H_2O.

CO chemisorption measurements were performed using a Micromeritics ASAP 2010C instrument. The samples were exposed to a flow of hydrogen for 1 h at 300, 450 or 600 °C, and then exposed to a flow of helium to cool down to 40 °C. Two chemisorption isotherms were measured at 40 °C using 5 vol% CO in He balance. First, the isotherm corresponding to all carbon monoxide (physi- and chemisorbed) on the catalyst was measured, and after evacuation at the same temperature for 1 h, the second one, corresponding to the weakly adsorbed CO.

2.3. Catalytic performance test

After the H_2 pretreatment, 75 mg of the catalyst powders was charged into a round-shaped glass flask with 1.5 mmol of BA in 1.5 mL of toluene. After purging the flask with pure N_2 at atmospheric pressure, the temperature was raised to 80 °C and the reaction initiated by switching the gas flow to pure O_2 for 1 h. The conversion and selectivity to BAL after 1h of reaction were determined using a gas chromatograph (Simadzu GC-14A) equipped with a flame ionization detector and Q-plot capillary column using an internal standard (*o*-dichlorobenzene). Identification of reaction products (BAL and benzoic acid) was also carried out by means of GC-MS (Shimadzu, GC-MS-QP5050A) and NMR (JEOL, JNM-ECA-600).

2.4. Preparation of catalyst layer

For in situ spectroscopic analyses, a thin film of the pretreated catalyst powder was prepared using the following procedure. A slurry consisting of 180 mg of catalyst and 24 mL of ethanol was first ultrasonicated for 30 min and then stirred overnight using a magnetic stirrer to achieve a uniform suspension. Subsequently, 1.6 mL of the slurry was placed on a ZnSe internal reflection element (IRE, bevel of 45°, 52mm x 20mm x 2mm) and the ethanol was evaporated at room temperature overnight. Prepared by this procedure, the catalyst layer adhered to the IRE such that no loss of catalyst was observed over the course of several hours under liquid flow–through conditions [40]. The catalyst deposited onto the IRE amounted to 12 ± 0.1 mg to ensure that the path of the evanescent wave was all covered by the catalyst layer.

2.5. Attenuated total reflection infrared (ATR-IR) and modulation-excitation spectroscopy (MES)

ATR-IR spectroscopy is a powerful tool to monitor catalytic solid-liquid interfaces [40, 41]. ATR–IR spectra were recorded on a Bruker Vertex 70 spectrometer equipped with a liquid nitrogen cooled MCT detector. A stainless-steel flow–through cell (total inner volume: 250 μL) mounted on an ATR–IR attachment (HARRICK) was used for all the transient adsorption-desorption measurements and reaction analyses. Spectra were recorded at 4 cm^{-1} resolution. The measurement temperature (25 °C or 80 °C) was regulated by a thermostat (Julabo, F25).

Modulation-excitation spectroscopy (MES) [42-45] was carried out by periodically switching between two different solutions. For the adsorption-desorption experiments, BA (1 mM) in toluene and pure toluene were filled into two separated glass-made bubble tanks where solutions were saturated sparging pure helium (99.99 % purity, 100 mL/min). The O_2-He modulation experiments of the aerobic oxidation were performed by switching between solutions of 1 mmol/L of BA in toluene saturated by sparging O_2 or He at a flow rate of 100 mL/min. The concentration of benzyl alcohol was low enough to avoid IR absorption bands assignable to BA in the liquid phase. The tanks were connected to the flow-through cell by Teflon tubings. Solutions were continuously admitted at a flow rate of 5.0 mL/min using a peristaltic pump (ISMATEC, Reglo 100) installed at the outlet of the cell. MES measurements of BA oxidation was performed at 80 °C in the liquid phase inside the cell. An automated 4-way valve (VICI Valco Instruments Co. Inc.) was synchronized with the acquisition of IR spectra by the spectrometer software (Bruker Optics, OPUS). Sixty spectra were recorded per cycle. The initial three cycles were used to stabilize the periodic response to reach a stable adsorption-desorption cycling. Afterward, six cycles were measured and averaged into a single cycle to enhance the signal-to-noise (S/N) ratio and the time resolution. The frequency of

modulation was fixed to 0.0025 Hz (400 s). Phase sensitive detection (PSD) was applied to remove the noise and to extract qualitative kinetic information. The acquired time-domain spectra were mathematically treated by PSD [46] to obtain phase-domain spectra according to the following equation:

$$A_k(\tilde{\nu})\cos\left(\varphi_k + \varphi_k^{delay}(\tilde{\nu})\right) = \frac{2}{T}\int_0^T A(t,\tilde{\nu})\sin\left(k\omega t + \varphi_k\right)\mathrm{d}t$$

where *T* is the length of a cycle, ω is the demodulation frequency (ω = 1 in this study), φk is the demodulation phase angle, *k* is the demodulation index (*k* = 1 in this study), and $A(t, \tilde{\nu})$ and $Ak(\tilde{\nu})$ are the active species responses in the time and phase domains, respectively. The above equation indicates that chemical events at a high in-phase angle, i.e., little phase delay, follow immediately after the changes in the liquid-phase or gas-phase, indicating that these processes, for example adsorption, occur rapidly. On the other hand, a low in-phase angle suggests that a process occurs slowly. All the phase-domain figures were expressed with relative absorbance. The time-domain spectra were employed to assign IR bands while the phase-domain spectra are being used for qualitative kinetic analysis of different surface species.

3. **Results and discussion**

3.1 Iridium supported on different metal oxides

Table 1 summarizes the BET surface areas, results of CO adsorption, and catalytic data of the benzyl alcohol oxidation at 80 ^{o}C. Reaction products detected were only BAL and benzoic acid for all the catalysts. The catalytic activity and selectivity followed the order Ir/TiO_2 > Ir/Al_2O_3 > Ir/CeO_2 in line with previous results [28]. Since the order of the BET surface areas does not obey the same trend, the surface area seems rather irrelevant for the catalytic activity. Figure 1 shows the TEM images of the differently supported 5%wt% Ir catalysts and the corresponding Ir particle size distributions. The Al_2O_3-supported catalyst showed the smallest mean size of the Ir particles (1.2 nm), while that on the CeO_2- and TiO_2-suported catalysts was significantly higher, 2.5 and 2.6 nm, respectively. Note that the determined mean Ir particle size and the corresponding catalytic activities and selectivities (Table 1) are obviously not correlated.

The ratio CO/Ir, defined as the amount of CO adsorbed per total amount of Ir atoms loaded, does not correlate with the catalytic performance either. Therefore, the strongly different catalytic behaviors of these catalysts have to be related to the nature of the support metal oxide. To unveil the reasons and underlying mechanisms of the observed support effects, in situ ATR-

IR spectroscopy in tandem with MES was employed for the aerobic oxidation of BA. MES is a powerful tool to remove IR signals of bulk solvent (toluene in this study) and to enhance the S/N ratio [43, 44]. Furthermore, mathematical processing of the data with PSD allows a qualitative kinetic evaluation by analyzing in-phase angle/phase-delay [44, 46]. Figures 2a-c and 2d-f show time-domain and phase-domain IR spectra recorded during adsorption-desorption of 1 mM of BA in toluene saturated with pure He at 25 ^{o}C on Ir/Al_2O_3, Ir/CeO_2, and Ir/TiO_2, respectively. For all the catalysts, IR bands assigned to BA were observed. Since the band features of BA differed from the ones of bulk BA in liquid phase (Figure S1, in Supplementary Material), the observed species in Figure 2 are considered to be adsorbed on the catalyst surface. The sharp absorption bands of BA at 1454 cm^{-1} (assigned to δ(C-H), ν(C-C), and the skeletal vibrations of benzene ring), 1208 cm^{-1} (ν(C-C)), 1007 cm^{-1} (ν(C-O) at 1100 and 1020 cm^{-1}) [37] emerged on the same time scale. Notably the band of ν(C-O) shifted to lower wavenumber for all the catalysts, compared to the corresponding one of the bulk BA in the liquid phase (Figure S1). Therefore, we infer that BA was dissociatively adsorbed on the catalyst surface through the oxygen atom forming the corresponding alkoxy species ($C_6H_5CH_2O$-), as speculated in previous studies. The absorbance scale considerably differed depending on the catalyst support; 0.0004 for Al_2O_3, 0.004 for CeO_2 and 0.001 for TiO_2, being indicative of the largest amount of adsorbed BA on the Ir/CeO_2 catalyst, though the BET surface area of this catalyst was the smallest (30 m^2/g), as listed in Table 1. As emerges from Figures 2d - 1f (phase-domain spectra), Ir/CeO_2 showed a higher in-phase angle (φ^{PSD} = 280 ^{o}) than the other catalysts. The high in-phase angle indicates rapid adsorption of BA and its strong interaction with the CeO_2 support. In contrast, Ir/Al_2O_3 and Ir/TiO_2 showed relatively slow adsorption of BA and weaker interaction with the catalysts. The too strong interaction of BA with CeO_2 could account for the low catalytic performance of Ir/CeO_2 (Table 1).

Figure 3 shows phase-domain (a-c) and time-domain (d-f) IR spectra during aerobic oxidation of BA on Ir/Al_2O_3 (a, d), Ir/CeO_2 (b, e) and Ir/TiO_2 (c, f) at 80 ^{o}C. The modulation experiments were carried out with 1 mmol/L of BA in toluene saturated with O_2 or He (O_2 - He modulation) to investigate the role of oxygen in the catalytic cycle. There are mainly three absorption bands observed: a bands at around 3420 cm^{-1}, assignable to perturbation of the hydroxyl groups of the support upon contact with adsorbed BA, a band at 1617 cm^{-1} indicative of skeletal vibrations of the aromatic ring, and one at 1081 cm^{-1} due to (ν(C-O) vibration of the adsorbed alkoxide, $C_6H_5CH_2O$-. These bands emerged when He-saturated BA solution was introduced, indicating the dissociative adsorption of BA on the surface, which is devoid of adsorbed oxygen. From the recorded spectra we infer that under the conditions used the

dissociative adsorption of BA is relatively slow and probably rate determining, whereas the second step, the oxidative dehydrogenation of the adsorbed alkoxide and desorption of BAL occurs more rapidly. Note that the rates of the two steps will be influenced by the surface concentrations of BA and O_2, and the state of the surface (reduced or oxidized) in this complex catalytic system, Therefore a prediction of the rate-determining step for steady-state aerobic oxidation cannot be given without considering the specific reaction conditions. At this point, it should be recalled that a critical parameter encountered with some platinum group metals is the oxygen supply rate, when it is higher than its consumption, surface metal atoms tend to be continuously oxidized and over-oxidized metal surfaces eventually deteriorate the catalytic activity [47-49]. On the other hand, too low oxygen concentration results in low catalytic performance. Therefore, there is a trade-off between high catalytic performance and oxygen poisoning of the active metal surface [50].

The transient adsorbed alkoxy species was only detectable on Ir/Al_2O_3 and Ir/TiO_2, and predominantly in the absence of O_2-saturated solution, as highlighted by the broad band at ca. 1080 cm^{-1}. A weak band at 1729 cm^{-1} assignable to the ν(C=O) stretching vibration of BAL was observed only for Ir/TiO_2 in the presence of O_2. Because Ir/TiO_2 showed the best catalytic performance, the produced BAL was abundant and could be detected on the surface. On Ir/Al_2O_3, such a band (ν(C=O)) was not detectable, in accord with the relatively poorer conversion and selectivity observed. With Ir/CeO_2 (Figure 3b), a weak band appeared at 2045 cm^{-1}, assigned to on-top CO adsorbed on metallic Ir particles. Thus, on Ir/CeO_2 the dissociative adsorption of BA concurred with the decomposition of BA leading to poor selectivity to BAL (Table 1). Furthermore, the spectra showed virtually no band due to ν(C-O) vibration of the adsorbed alkoxide ($C_6H_5CH_2O$-).

Evidence for the adsorbed transient alkoxy species during the aerobic oxidation of an alkyl alcohol, 2-propanol, over Pd/Al_2O_3, has earlier been reported by Bürgi and Bieri [51, 52], using also MES in combination with ATR-IR spectroscopy. They switched the feed in the modulation experiments periodically between hydrogen- and oxygen-saturated solutions of 2-propanol. Consequently, in their experiments the state of the catalyst surface was driven fast between reduced and oxidized states, which significantly differs from the modulation applied in our study, where between He- and O_2-saturated solutions was switched. Their experiments showed that the dissociative adsorption of the alcohol is relatively fast, whereas its further oxidative dehydrogenation to the aldehyde is slow and rate-determining. This stands in contrast to our observation and clearly demonstrates that the relative rates of the two reaction steps are strongly influenced by the conditions, as discussed above. However, in practice the aerobic

alcohol oxidation is not carried out with hydrogen in the feed and thus the conditions they used are quite far from those encountered in continuous aerobic oxidation of alcohols. With their experimental strategy, modulating between solutions of the alcohol solution saturated with H_2 and O_2, it is likely that the dissociative adsorption of the alcohol is much faster than in our case, where a He-saturated solution of the alcohol is used, because the catalyst surface is more efficiently freed from adsorbed oxygen blocking the active metal sites. Note that there is considerable evidence that the active catalytic sites are in the metallic state (M^o) [3, 47, 53, 54]. It has earlier been shown that the rate of alcohol dehydrogenation is much faster on a reduced metal surface than on an oxidized one [55], Overall, we can conclude that the use of H_2 instead of an inert gas (He) has a significant effect on the dynamic of the surface processes. Nevertheless, in both studies, irrespective of the altered experimental procedure, leading to different states of the catalysts, the transient adsorbed alkoxide species was detected. This detection is hardly possible by steady-state experimentation, which underlines the importance of transient methods for the investigations of reaction intermediates.

To our knowledge the presence of a transient adsorbed alkoxide has so far not been verified for the aerobic oxidation of an aromatic alcohol on supported Ir catalysts. Here we have evidenced that in the aerobic oxidation of an aromatic alcohol the key to high catalytic performance is also the dissociative adsorption of the alcohol, that is the formation of the adsorbed alkoxide intermediate, as earlier proposed for alkyl alcohols. This could not inevitably be expected since the adsorption behavior and reactivity of aromatic alcohols is generally different compared to that of simple alkyl alcohols [3, 56].

3.2 Iridium supported on titania pretreated in hydrogen at different temperature

In order to gain deeper insight into the effect of SMSI observed with Ir nanoparticles deposited on titania, samples, 2wt% Ir/TiO_2 catalysts were pretreated at 300, 450 and 600 ^oC under H_2 flow for 3h. These samples were then characterized by nitrogen (BET), and CO adsorption measurements, TEM, and subjected to catalytic tests. TEM images and corresponding Ir particle size distributions of the differently pretreated Ir/TiO_2 samples are presented in Figure 4. As expected, the Ir particle size remained almost the same (1.6 – 1.8 nm), even after H_2 treatment at elevated temperature (600 ^oC), confirming earlier TEM investigations [29, 57, 58]. Therefore, the particle size of Ir seems to be virtually irrelevant for explaining the different catalytic behaviors of the Ir/TiO_2 catalysts pretreated in hydrogen at different temperature (Table 1). The BET surface area decreased only little for the catalyst pretreated at 450 ^oC, but significantly for the one pretreated at 600 ^oC. Most striking was the

effect of the pretreatment temperature on the CO/Ir ratio, which dropped from 0.68 for the sample pretreated at 300 °C to 0.0 for the sample pretreated at 600 °C (Table 1). This indicates that the strong-metal-support-interaction (SMSI), resulting in covering the Ir particle surface with a thin layer of partially reduced titania, was progressively increasing with higher temperature of the hydrogen pretreatment, and finally completely covered the Ir particle surface.

Interestingly, Ir/TiO_2 pretreated at 450°C showed the best catalytic performance in terms of conversion, turnover frequency (TOF), and selectivity, even though most of the Ir surface was covered by the partially reduced TiO_2 layer. Ir/TiO_2 (450°) showed a more than seven times higher catalytic performance than Ir/TiO_2 (300°C), though the molecular CO/Ir ratio decreased by a factor of ca. 4 (0.68 to 0.16), as shown in Table 1. Most astonishingly, there was no CO adsorption observed for Ir/TiO_2 (600°C), which however still showed relatively high catalytic activity and selectivity (Table 1). In this case, the surface of Ir particles is completely covered by partially reduced titania and is not accessible for CO adsorption and thus also not for BA. Since there was no catalytic activity observed with the pure TiO_2 support pretreated with H_2 at 600 °C, the partially reduced TiO_x covering the Ir particles is considered to be catalytically active.

To gain deeper insight into the effect caused by the SMSI, we carried out ATR-IR-MES experiments to examine the adsorption-desorption of BA at 25 °C. The lower temperature was chosen to avoid any possible disturbing side reaction, such as the disproportionation of adsorbed BA species forming carbon monoxide adsorbed on the metal particles [34]. Figure 5 shows time-domain (a-c) and phase-domain (d-f) spectra. As expected, the absorbance of BA dramatically decreased with the temperature of H_2 pretreatment. However, even for Ir/TiO_2 (600 °C), a small amount of adsorbed alkoxide ($C_6H_5CH_2O$-) was detected, in spite of the fact that no CO chemisorption could be detected on the Ir particles (Table 1). Compared to the liquid phase spectrum of pure benzyl alcohol (Figure S1), the band of the *v* (C-O) stretching vibration split into two bands, one of which is located at a higher wavenumber at ca. 1040 cm^{-1}. The original band at 1016 cm^{-1} is assigned to adsorbed alkoxide species (benzyloxy) bound to the metal surface (Ir), while bands at higher wavenumber originate from alkoxide adsorbed on metal cations of the titania overlayer due to oxygen vacancies [59]. The H_2 pretreatment at high temperature leads to a reduction of TiO_2 to TiO_x in the titania layer covering the Ir particles [29, 36]. Therefore, it is reasonable to assume that the alkoxide ($C_6H_5CH_2O$-) adsorbs on the Ti cations with oxygen vacancies in the layer covering the Ir nanoparticles. This formation of the transient adsorbed alkoxide ($C_6H_5CH_2O$-) intermediate is likely the reason for the

unexpected catalytic activity of Ir/TiO_2 (600°C), which does not expose any accessible Ir surface. The in-phase angle of the adsorbed alkoxide was the highest for Ir/TiO_2 (450°C), which implies that the facile formation of the alkoxide on the surface is also key for high catalytic performance in this catalysts.

Figure 6 displays phase-domain (a-c) and time-domain (d-f) IR spectra during aerobic oxidation of BA on Ir/TiO_2 (300 °C) (a, d), Ir/TiO_2 (450 °C) (b, e), and Ir/TiO_2 (600 °C) (c, f) at 80 °C. The experimental conditions for O_2 - He modulation are the same as those in Figure 3. However, 2 wt% Ir/TiO_2 showed much lower absorbance, which further decreased with the H_2 pretreatment temperature. The formation of adsorbed alkoxide species, indicated by the band at 1098 cm^{-1} (highlighted in blue in Figures 6d-6e) occurred at similar timing in the absence of O_2 (200 – 400 s). However, the further reaction of the transient alkoxide significantly depended on the temperature of H_2 reduction. The alkoxide band disappeared completely after 142 s for Ir/TiO_2 (300 °C) while it took only 95 s for Ir/TiO_2 (600 °C). Thus the Ir particles completely covered by the titania overlayer enhanced the second oxidative dehydrogenation, that is the reaction of the intermediate alkoxide to BAL. A new band at 1098 cm^{-1} emerged due to the formation of on-top alkoxy species on the metal cation of the titania support [59]. The oxygen vacancy of Ti cations seems to be filled with the adsorbed alkoxy species ($C_6H_5CH_2O$-) to balance the charge. Water molecules adsorbed on the surface were also detected appearing as a broad band centered at 1624 cm^{-1}. Taking all the findings into account, we propose the following reaction mechanism: BA adsorbs dissociatively on either Ir or TiO_x (Ti cations with oxygen vacancies) to form the transient adsorbed alkoxide ($C_6H_5CH_2O$-), which than in the presence of oxygen relatively quickly reacts to benzaldehyde and desorbs. Under the given conditions, the dissociative adsorption of BA generating the corresponding adsorbed alkoxide is relatively slow, whereas its further oxidative dehydrogenation to benzaldehyde and its desorption is fast. A competitive hydrogenation BAL → BA (backward reaction) cannot be ruled out if sufficient hydrogen, originating from the dissociative adsorption of BA, is formed during the period with He-saturated BA solution. Its significance depends on the relative rates of oxidative dehydrogenation (producing BAL and H_2O) and hydrogenation of BAL to BA.

There have been a number of reports on in situ IR studies on reaction mechanisms over different metal catalysts (e.g. Pd, Ru, Au) but they virtually all focused on monitoring the processes leading to by-products through decarbonylation and further oxidation to benzoic acid [35, 37-39]. To our knowledge the present study is the first proving the pivotal role of the adsorbed transient alkoxy species in the aerobic oxidation of an aromatic alcohol. A similar

scenario seems also likely for the aerobic oxidation of other primary aromatic alcohols, where the formation of the adsorbed alkoxide is feasible and not sterically hindered.

4. Conclusions

We studied the effects of the support material and SMSI phenomenon for the oxidation of BA to BAL on Ir particles of 1.2 – 2.6 nm deposited on Al_2O_3, CeO_2, and TiO_2 supports. Depending on the nature of the support, the Ir catalysts showed very different catalytic performance obeying the order $Ir/TiO_2 > Ir/Al_2O_3 > Ir/CeO_2$. The lowest catalytic performance observed for the CeO_2-supported Ir catalyst is ascribed to the strong adsorption of BA on the ceria surface leading to its stabilization and deactivation. The dissociative adsorption of BA to form the corresponding transient alkoxide ($C_6H_5CH_2O$-) was confirmed on TiO_2- and Al_2O_3-supported Ir catalysts but not on Ir/CeO_2. The formation of alkoxide species is shown to be crucial for high catalytic performance and is relatively slow under the conditions used, while its further oxidative dehydrogenation occurred more rapidly. The SMSI observed with titania-supported Ir-catalysts promotes the formation of a reduced TiO_x layer covering the Ir nanoparticles and Ti cations with abundant oxygen vacancies. In spite of this blocking of Ir sites, the adsorbed transient alkoxide could still be formed, even on an Ir surface completely covered with reduced titania, as achieved after temperature pretreatment with hydrogen at 600 ^oC. The transient alkoxide ($C_6H_5CH_2O$-) is in this case adsorbed and further dehydrogenated on the reduced titania overlayer, covering the Ir nanoparticles, likely on the Ti cations with oxygen vacancies. This scenario accounts for the high catalytic activity of Ir/TiO_2 catalysts in the state of SMSI. MES-ATR-IR proved to be a valuable method giving access to the detection of reaction intermediates adsorbed at the catalytic liquid-solid interface.

5. Acknowledgement

This work was financially supported by the Natural Science Foundation of China (NSFC) (No. 21377017), the start-up grant from Dalian University of Technology (Nos. DUT13RC(03)04 and DUT13RC(3)26), the National Thousand Talents Program of China and the Fundamental Research Funds for the Central Universities of China.

Appendix A. Supplementary material

Supplementary data to this article can be found online at …

References

[1] R.A. Sheldon, I. Arends, G.J. Ten Brink, A. Dijksman, Green, catalytic oxidations of alcohols, Acc. Chem. Res. 35 (2002) 774-781.

[2] T. Matsumoto, M. Ueno, N. Wang, S. Kobayashi, Recent advances in immobilized metal catalysts for environmentally benign oxidation of alcohols, Chem. Asian J. 3 (2008) 196 – 214.

[3] T. Mallat, A. Baiker, Oxidation of alcohols with molecular oxygen on solid catalysts, Chem. Rev. 104 (2004) 3037-3058.

[4] C. P. Vinod, K. Wilson, A. F. Lee, Recent advances in the heterogeneously catalysed aerobic selective oxidation of alcohols, J. Chem. Technol. Biotechnol. 86 (2011) 161–171.

[5] C.E. Chan-Thaw , A. Savara, A. Villa, Selective benzyl alcohol oxidation over Pd catalysts, Catalysts 8 (2018) 431; doi:10.3390/catal8100431.

[6] X.D. Jiang, H. Liu, H.F. Liang, G.X. Jiang, J.L. Huang, Y.L. Hong, D.P. Huang, Q.B. Li, D.H. Sun, Effects of biomolecules on the selectivity of biosynthesized Pd/MgO catalyst toward selective oxidation of benzyl alcohol, Ind. Eng. Chem. 53 (2014) 19128-19135.

[7] L. Li, J.B. Zhao, J.Y. Yang, T. Fu, N.H. Xue, L.M. Peng, X.F. Guo, W.P. Ding, A sintering-resistant Pd/SiO_2 catalyst by reverse-loading nano iron oxide for aerobic oxidation of benzyl alcohol, RSC Adv. 5 (2015) 4766-4769.

[8] Q. Wang, X.C. Cai, Y.Q. Liu, J.Y. Xie, Y. Zhou, J. Wang, Pd nanoparticles encapsulated into mesoporous ionic copolymer: Efficient and recyclable catalyst for the oxidation of benzyl alcohol with O_2 balloon in water, Appl. Catal. B-Environ. 189 (2016) 242-251.

[9] P. Weerachawanasak, G.J. Hutchings, J.K. Edwards, S.A. Kondrat, P.J. Miedziak, P. Prasertham, J. Panpranot, Surface functionalized TiO_2 supported Pd catalysts for solvent-free selective oxidation of benzyl alcohol, Catal. Today 250 (2015) 218-225.

10] Q.L. Wei, T.J. Liu, Y.Y. Wang, L.Y. Dai, Three-dimensional N-doped graphene aerogel-supported Pd nanoparticles as efficient catalysts for solvent-free oxidation of benzyl alcohol, RSC Adv. 9 (2019) 9620-9628.

[11] Y. Hui, S. Zhang,W. Wang,, Recent progress in catalytic oxidative transformations of alcohols by supported gold nanoparticles, Adv. Synth. Catal. 361 (2019) 2215 – 2235.

[12] A.J. Faqeeh, T.T. Ali, S.N. Basahel, K. Narasimharao, Nanosized samarium modified Au-$Ce_{0.5}Zr_{0.5}O_2$ catalysts for oxidation of benzyl alcohol, Mol. Catal. 456 (2018) 10-21.

[13] C. Della Pina, E. Falletta, L. Prati, M. Rossi, Selective oxidation using gold, Chem. Soc. Rev. 37 (2008) 2077–2095.

[14] P. Haider, B. Kimmerle, F. Krumeich, W. Kleist, J-D. Grunwaldt, A. Baiker, Gold-catalyzed aerobic oxidation of benzyl alcohol: Effect of gold particle size on activity and

selectivity in different solvents, Catal. Letters 125 (2008) 169–176.

[15] A. S. Sharma, H. Kaur, D. Shah, Selective oxidation of alcohols by supported gold nanoparticles: Recent advances, RSC Adv. 6 (2016) 28688–28727.

[16] D. I. Enache, J. K. Edwards, P. Landon, B. Solsona-Espriu, A. F. Carley, A. A. Herzing, M. Watanabe, C. J. Kiely, D. W. Knight, G. J. Hutchings, Solvent-free oxidation of primary alcohols to aldehydes using Au-Pd/ TiO_2 catalysts, Science , 311 (2006) 362-365.

[17] V.V. Torbina, A.A. Vodyankin, S. Ten , G.V. Mamontov, M. A. Salaev, V. I. Sobolev, O. V. Vodyankina, Ag-based catalysts in heterogeneous selective oxidation of alcohols: A review, Catalysts 8 (2018) 447; doi:10.3390/catal8100447

[18] M. J. Beier, T.W. Hansen, J-D. Grunwaldt, Selective liquid-phase oxidation of alcohols catalyzed by a silver-based catalyst promoted by the presence of ceria, J. Catal. 266 (2009) . 320-330

[19] J.J. Liu, S.H. Zou, J.C. Wu, H. Kobayashi, H.T. Zhao, J. Fan, Green catalytic oxidation of benzyl alcohol over Pt/ZnO in base-free aqueous medium at room temperature, Chin. J. Catal. 39 (2018) 1081-1089.

[20] M.S. Ide, D.D. Falcone, R.J. Davis, On the deactivation of supported platinum catalysts for selective oxidation of alcohols, J. Catal. 311 (2014) 295–305.

[21] J. Liu, F. Han, L. Chen, L. Lu, S. Zou, H. Zhao, Remarkable promoting effects of BiOCl on the room-temperature selective oxidation of benzyl alcohol over supported Pt catalyst, New J. Chem. 42, (2018) 8979-8984.

[22] N. Dimitratos , A. Villa, D. Wang, F. Porta, D. Su , L. Prati, Pd and Pt catalysts modified by alloying with Au in the selective oxidation of alcohols, J. Catal. 244 (2006) 113–121.

[23] S. Marx, A. Baiker, Beneficial interaction of gold and palladium in bimetallic catalysts for the selective oxidation of benzyl alcohol, J. Phys. Chem. C 113 (2009) 6191-6201.

[24] M. Sankar, N. Dimitratos, P. J. Miedziak, P.P. Wells, C. J. Kiely, G. J. Hutchings, Designing bimetallic catalysts for a green and sustainable future, Chem. Soc. Rev. 41 (2012) 8099–8139.

[25] J.Y. Sun, Y.X. Han, H.Y. Fu, X.L. Qu, Z.Y. Xu, S.R. Zheng, Au@Pd/TiO_2 with atomically dispersed Pd as highly active catalyst for solvent-free aerobic oxidation of benzyl alcohol, Chem. Eng. J. 313 (2017) 1-9.

[26] P.P. Wu, Y.X. Cao, L.M. Zhao, Y. Wang, Z.K. He, W. Xing, P. Bai, S. Mintova, Z.F. Yan, Formation of PdO on Au-Pd bimetallic catalysts and the effect on benzyl alcohol oxidation, J. Catal. 375 (2019) 32-43.

[27] P.P. Wu, Y.X. Cao, L.M. Zhao, Y. Wang, Z.K. He, W. Xing, P. Bai, S. Mintova, Z.F. Yan,

Formation of PdO on Au-Pd bimetallic catalysts and the effect on benzyl alcohol oxidation, J. Catal. 375 (2019) 32-43.

[28] A. Yoshida, Y. Takahashi, T. Ikeda, K. Azemoto, S. Naito, Catalytic oxidation of aromatic alcohols and alkylarenes with molecular oxygen over Ir/TiO_2, Catal. Today 164 (2011) 332-335.

[29] A. Yoshida, Y. Mori, T. Ikeda, K. Azemoto, S. Naito, Enhancement of catalytic activity of Ir/TiO_2 by partially reduced titanium oxide in aerobic oxidation of alcohols, Catal. Today 203 (2013) 153-157.

[30] T-R. Chen, Y-X. Wang, W-J. Lee, K. H.-C. Chen, J-D. Chen, A reduced graphene oxide-supported iridium nanocatalyst for selective transformation of alcohols into carbonylcompounds via a green process, Nanotechnology 31 (2020) 285705.

[31] J. K. Mobley, M. Crocker, Catalytic oxidation of alcohols to carbonyl compounds over hydrotalcite and hydrotalcite supported catalysts, RSC Adv. 5 (2015) 65780-65797

[32] S.J. Tauster, S.C. Fung, R.L. Garten, Strong metal-support interactions - group 8 noble metals supported on TiO_2, J. Am. Chem. Soc. 100 (1978) 170-175.

[33] A.Villa, D. Ferri, S. Campisi, C.E.Chan-Thaw, Y. Lu, O. Kröcher, L. Prati, Operando Attenuated Total Reflectance FTIR Spectroscopy: Studies on the Different Selectivity Observed in Benzyl Alcohol Oxidation. ChemCatChem 7 (2015) 2534 – 2541.

[34] D. Ferri, A. Baiker, Advances in infrared spectroscopy of catalytic solid-liquid interfaces: The case of selective alcohol oxidation, Top. Catal. 52 (2009) 1323-1333.

[35] D. M. Meier, A. Urakawa, A. Baiker, In situ PM-IRRASs study of liquid-phase benzyl alcohol oxidation on palladium, J. Phys. Chem. C 113 (2009) 21849–21855.

[36] D. Ferri, C. Mondelli, F. Krumeich, A. Baiker, Discrimination of active palladium sites in catalytic liquid-phase oxidation of benzyl alcohol, J. Phys Chem. B, 110 (2006) 22982-22986.

[37] C. Keresszegi, D. Ferri, T. Mallat, A. Baiker, Unraveling the surface reactions during liquid-phase oxidation of benzyl alcohol on Pd/Al_2O_3: an in situ ATR-IR study, J. Phys. Chem. B 109 (205) 958-967.

[38] C. Mondelli, D. Ferri, A. Baiker, Ruthenium at work in Ru-hydroxyapatite during the aerobic oxidation of benzyl alcohol: An in situ ATR-IR spectroscopy study, J. Catal., 258 (2008) 170-176.

[39] C. Mondelli, D. Ferri, J.D. Grunwaldt, F. Krumeich, S. Mangold, R. Psaro, A. Baiker, Combined liquid-phase ATR-IR and XAS study of the Bi-promotion in the aerobic oxidation of benzyl alcohol over Pd/Al_2O_3, J. Catal. 252 (2007) 77-87.

[40] T. Bürgi, A. Baiker, Attenuated total reflection infrared spectroscopy of solid catalysts functioning in the presence of liquid-phase reactants, In *Advances in Catalysis*; Gates, B.C., Knözinger, H., Eds; Elsevier: Amsterdam, The Netherlands, 2006; Volume 50, pp. 227–283.

[41] J.M. Andanson, A. Baiker, Exploring catalytic solid/liquid interfaces by in situ attenuated total reflection infrared spectroscopy, Chem. Soc. Rev. 39 (2010) 4571-4584.

[42] D. Baurecht, U.P. Fringeli, Quantitative modulated excitation Fourier transform infrared spectroscopy, Rev. Sci. Instrum. 72 (2001) 3782-3792.

[43] T. Bürgi, A. Baiker, In situ infrared spectroscopy of catalytic solid-liquid interfaces using phase-sensitive detection: Enantioselective hydrogenation of a pyrone over Pd/TiO_2, J. Phys. Chem. B 106 (2002) 10649-10658.

[44] A. Urakawa, T. Bürgi, A. Baiker, Sensitivity enhancement and dynamic behavior analysis by modulation excitation spectroscopy: Principle and application in heterogeneous catalysis, Chem. Eng. Sci. 63 (2008) 4902-4909.

[45] P. Mueller, L. Hermans, Applications of modulation excitation spectroscopy in heterogeneous catalysis, Ind. Eng. Chem. 56 (2017) 1123-1136.

[46] D. Baurecht, I. Porth, U.P. Fringeli, A new method of phase sensitive detection in modulation spectroscopy applied to temperature induced folding and unfolding of RNase A, Vib. Spectrosc. 30 (2002) 85-92.

[47] T. Mallat, A. Baiker, Catalyst Potential - a Key for Controlling Alcohol Oxidation in Multiphase Reactors. Catal. Today 24 (1995) 143-150.

[48] T. Mallat, A. Baiker, Oxidation of alcohols with molecular-oxygen on platinum metal catalysts in aqueous-solutions. Catal. Today 19 (1994) 247-283.

[49] M. Besson, P. Gallezot, Selective oxidation of alcohols and aldehydes on metal catalysts. Catal. Today 57 (2000) 127-141.

[50] T. Mallat, Z. Bodnar, C. Brönnimann, A. Baiker, Platinum-catalyzed oxidation of alcohols in aqueous-solutions - the role of Bi-promotion in suppression of catalyst deactivation; Elsevier Science Publ B V: Amsterdam, 1994; Vol. 88, p 385-392.

[51] T. Bürgi, M. Bieri, Time-resolved in situ ATR spectroscopy of 2-propanol oxidation over Pd/Al_2O_3: Evidence for 2-propoxide intermediate, J. Phys. Chem. B 108 (2004) 13364-13369.

[52] T. Bürgi, Combined in situ attenuated total reflection infrared and UV-vis spectroscopic study of alcohol oxidation over Pd/Al_2O_3, J. Catal. 229 (2005) 55-63.

[53] E. Müller, K. Schwabe, Oxidation of watery ethyl alcohol with molecular oxygen catalysed by platinum metals, Kolloid-Z. 52 (1930) 163-173.

[54] R. DiCosimo, G.M. Whitesides, Oxidation of 2-propanol to aceton by dioxygen on a platinized electrode under open-circuit conditions, J. Phys. Chem. 93 (1989), 768-775.

[55] J. M. H. Dirkx, H.S. van der Baan, M. A. J. J. van den Broen, Preparation of D-glucaric acid by oxidation of D-gluconic acid-catalyzed by platinum on carbon, Carbohydrate Research, 59 (1977) 63-72.

[56] T. Mallat, A. Baiker, Asymmetric catalysis at chiral metal surfaces, Chem. Rev. 107 (2007) 4863-4890.

[57] X.Y. Shi, W. Zhang, C. Zhang, W.T. Zheng, H. Chen, J.G. Qi, Real-space observation of strong metal-support interaction: state-of-the-art and what's the next, J. Microsc. 262 (2016) 203-215.

[58] H. Iddir, M.M. Disko, S. Ogut, N.D. Browning, Atomic scale characterization of the Pt/TiO_2 interface, Micron 36 (2005) 233-241.

[59] J.H. Jhang, A. Schaefer, V. Zielasek, J.F. Weaver, M. Baumer, Methanol adsorption and reaction on samaria thin films on Pt(111), Materials 8 (2015) 6228-6256.

Captions of Table and Figures

Table 1. Textural properties and catalytic performance of differently supported Ir/metal oxide catalysts. The reaction conditions are given in the experimental section.

Figure 1. TEM images and size distribution histograms of Ir particles of (a, d) 5 wt% Ir/Al_2O_3, (b, e) 5 wt% Ir/CeO_2, (c,f) Ir/TiO_2

Figure 2. (a-c) Time-domain and (d-f) phase-domain IR spectra recorded during adsorption-desorption of BA in toluene on (a, d) 5 wt% Ir/Al_2O_3, (b, e) 5 wt% Ir/CeO_2, (c, f) 5 wt% Ir/TiO_2 at 25 ^oC. The unit of z-axis for the phase-domain spectra is relative absorbance.

Figure 3. (a-c) Phase-domain and (d-f) time-domain IR spectra recorded during aerobic oxidation of BA on (a, d) 5 wt% Ir/Al_2O_3, (b, e) 5 wt% Ir/CeO_2, (c, f) 5 wt% Ir/TiO_2 at 25 ^oC.

Figure 4. TEM images and size distribution histograms of Ir particles of 2 wt% Ir/TiO_2 catalysts after pre-treatment with hydrogen at different temperatures for 3h; (a, d) Ir/TiO_2 (300), (b, e) Ir/TiO_2 (450), (c, f) Ir/TiO_2 (600). Temperatures of pretreatments in ^oC are indicated in parentheses.

Figure 5. (a-c) Time-domain and (d-f) phase-domain IR spectra recorded during adsorption-desorption of 1 mmol/L of BA in toluene on (a, d) 2 wt% Ir/TiO_2 (300), (b, e) 2 wt% Ir/TiO_2 (450), (c, f) 2 wt% Ir/TiO_2 (600) at 25 ^oC. The unit of z-axis for the phase-domain spectra is relative absorbance.

Figure 6. (a-c) Phase-domain and (d-f) time-domain IR spectra recorded during aerobic oxidation of BA on on (a, d) 2 wt% Ir/TiO_2 (300), (b, e) 2 wt% Ir/TiO_2 (450), (c, f) 2 wt% Ir/TiO_2 (600) at 25 ^oC.

Catalyst	BET surface area (m^2/g)	CO/Ir [a]	Conversion (%)	Mean TOF [b] (h^{-1})	Selectivity to BAL (%)
5 wt% Ir/Al_2O_3	119	0.50	23	35	79
5 wt% Ir/CeO_2	30	0.78	10	10	69
5 wt% Ir/TiO_2	58	0.50	77	118	98
2 wt% Ir/TiO_2 (300)	64	0.68	42	119	98
2 wt% Ir/TiO_2 (450)	60	0.16	69	829	> 99
2 wt% Ir/TiO_2 (600)	39	0.00	32	n.d.	> 99

[a]The ratio of CO molecules adsorbed to the total amount of iridium atoms exposed on the surface.

[b]Mean turnover frequency per surface Ir atom derived from the conversion of BA after 1h of reaction. The determination of the number of the surface Ir atoms is based on the assumption that one CO molecule adsorbs on one surface Ir atom (stoichiometric factor = 1).

Table 1

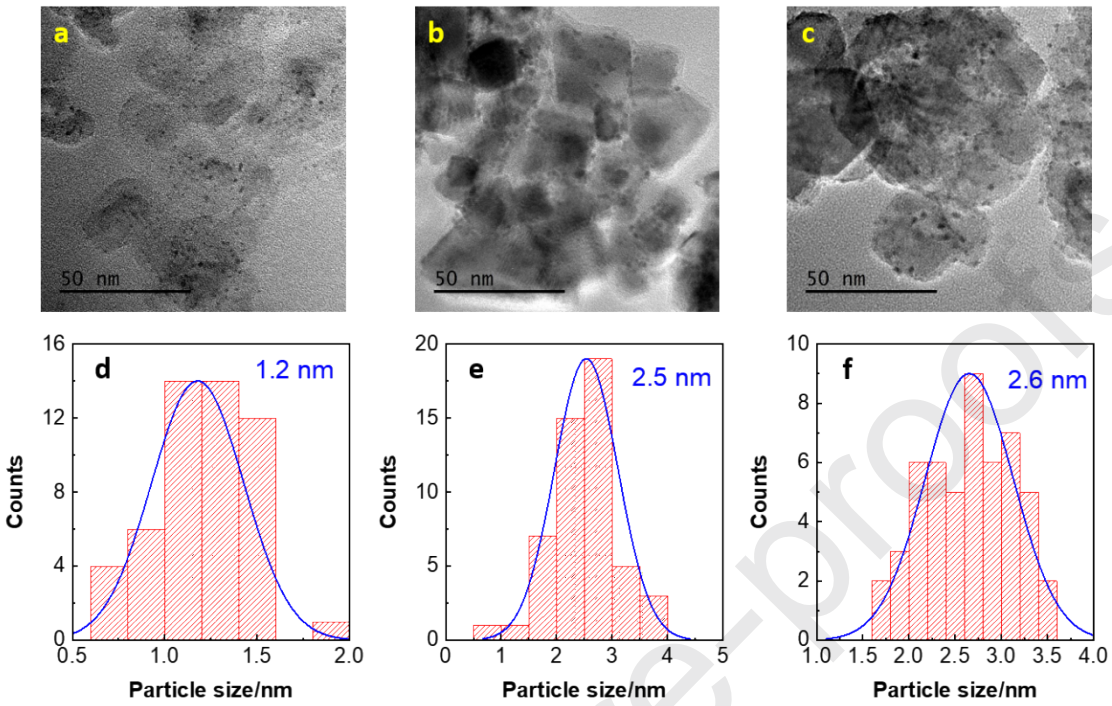

Figure 1

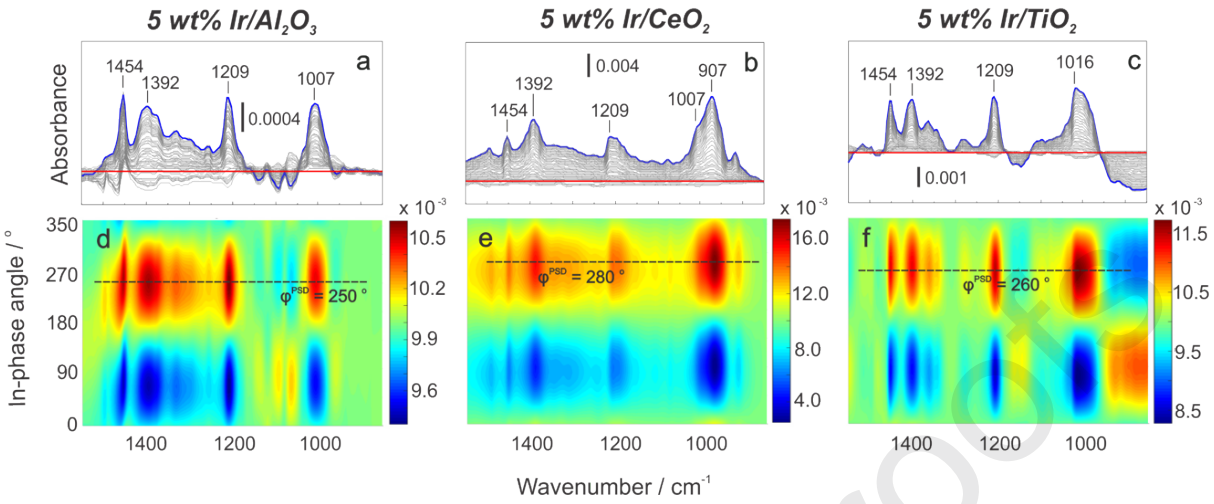

Figure 2

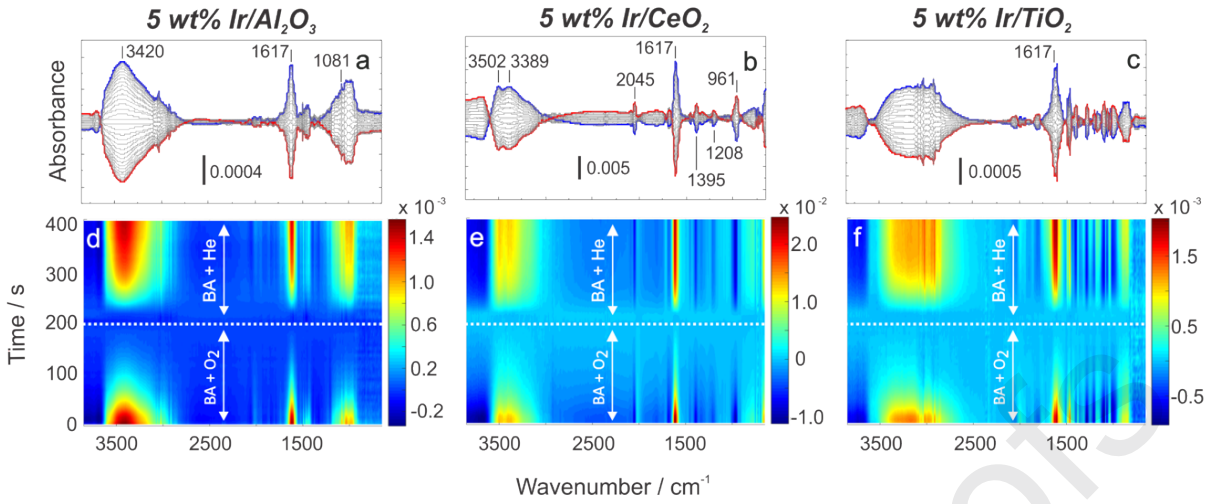

Figure 3

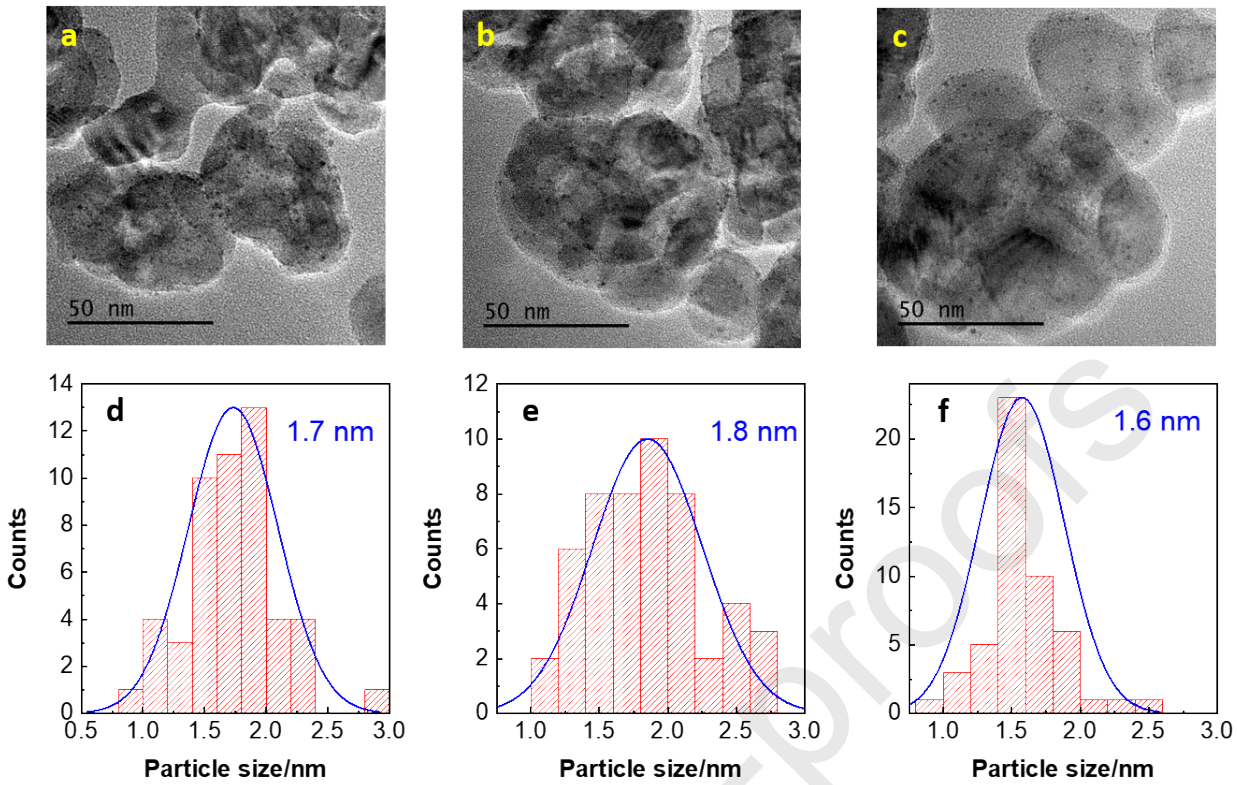

Figure 4

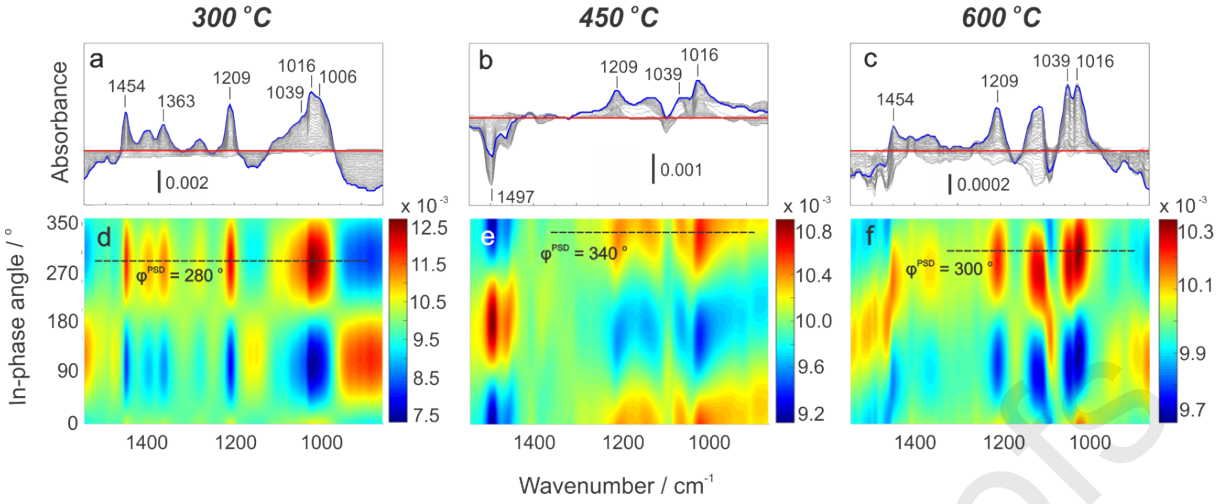

Figure 5

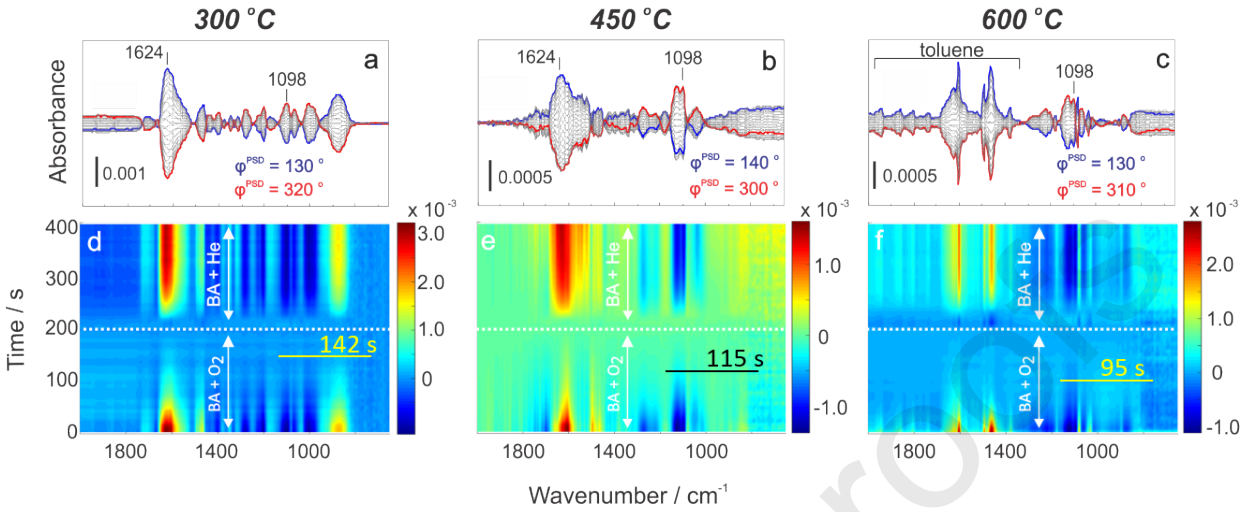

Figure 6

Graphical abstract